AAS 20-562

ECLIPSE AVOIDANCE IN DYNAMICAL STRUCTURES NEARBY NRHOS IN A HIGHER-FIDELITY MODEL

Emily M. Zimovan-Spreen[*], Kathleen C. Howell[†], and Diane C. Davis[‡]

A dynamical understanding of orbits in the Earth-Moon neighborhood, particularly in the vicinity of the NRHOs, is relevant to future long-duration missions in this region. Power, thermal, and line of sight constraints dictate allowable eclipsing conditions for spacecraft. In response, characteristics of significant dynamical structures nearby the NRHOs, including eclipse-avoidance properties, are verified in a higher-fidelity ephemeris model. An eclipse avoidance strategy, based on resonance with the lunar synodic period and the incorporation of a path constraint within a targeting scheme, is developed and verified. As a result, long-duration, eclipse-free trajectory solutions in a higher-fidelity model are constructed.

INTRODUCTION

An enduring human presence in the regions beyond Low Earth Orbit (LEO) is viewed by NASA and a variety of private organizations as an essential step in the development of a robust space economy and the evolution of crewed missions to Mars. A dynamical understanding of orbits in the Earth-Moon neighborhood that can sustain long-term activities and a network of trajectories that link locations of interest forms a critical foundation for the creation of an infrastructure to support a lasting human presence. The Gateway, a future long-term habitat or hub in an orbit near the Moon, is expected to serve as a staging location for activities and missions within cislunar space. Currently, the orbit of interest for a habitat in cislunar space is a Near Rectilinear Halo Orbit (NRHO).[1]

Analysis by Zimovan-Spreen and Howell in the circular restricted three-body problem (CR3BP) demonstrates that structures bifurcating from the NRHO region along the L_2 halo orbit family offer insight into the flow in the vicinity of the NRHOs.[2] Limitations on eclipse duration for spacecraft in cislunar space arise from power and thermal requirements, thus, innovative strategies to avoid frequent and long-duration eclipses are necessary to meet mission constraints.[3,4] In this investigation, dynamical structures nearby the NRHOs are explored and the characteristics of these nearby related orbits, including eclipse-avoidance properties, are highlighted and, subsequently, verified in a higher-fidelity ephemeris model. A strategy is explored that is based on orbits in resonance with the lunar synodic period combined with careful epoch selection. Additionally, a strategy to enforce an eclipse avoidance constraint within a targeting scheme is developed and verified. This approach allows both Earth and Moon eclipses to be avoided over a long duration without significant propellant requirements.

DYNAMICAL MODELS

Circular Restricted Three-Body Problem

The dynamical model in the CR3BP serves as a reasonable approximation to the higher-fidelity dynamical models in the Earth-Moon system, including those that may also incorporate solar gravity. Within this application of the CR3BP, the motion of a massless spacecraft under the gravitational influence of the Earth and Moon is explored. These two primary bodies, modeled as point-masses, are assumed to move in circular

[*]Ph.D. Candidate, School of Aeronautics and Astronautics, Purdue University, 701 W. Stadium Avenue, West Lafayette, IN 47907-2045
[†]Hsu Lo Distinguished Professor of Aeronautics and Astronautics, Purdue University, 701 W. Stadium Avenue, West Lafayette, IN 47907-2045
[‡]Principal Systems Engineer, a.i. solutions, Inc., 2224 Bay Area Blvd., Houston, TX 77058

orbits about their common barycenter. The motion of the spacecraft is then described relative to a coordinate frame, $\hat{x}$-$\hat{y}$-$\hat{z}$, that rotates with the motion of the Earth and Moon. The position vector of the spacecraft relative to the system barycenter is written as $\mathbf{r}_{Bsc} = x\hat{x} + y\hat{y} + z\hat{z}$. Expressed in the rotating frame, the scalar equations of motion for the spacecraft are then written as

$$\ddot{x} - 2\dot{y} = \frac{\partial U}{\partial x},\ \ddot{y} + 2\dot{x} = \frac{\partial U}{\partial y},\ \ddot{z} = \frac{\partial U}{\partial z} \tag{1}$$

where the pseudo-potential function, $U = \frac{1}{2}(x^2 + y^2) + \frac{1-\mu}{d_1} + \frac{\mu}{d_2}$, while $d_1 = \sqrt{(x+\mu)^2 + y^2 + z^2}$, and $d_2 = \sqrt{(x-1+\mu)^2 + y^2 + z^2}$. The CR3BP admits five relative equilibrium points: the collinear points L_1, L_2, and L_3, located along the Earth-Moon line, and two equilateral points, L_4 and L_5, that form equilateral triangles with the two primaries. An energy-like integral of the motion, denoted the Jacobi constant, exists in the rotating frame such that $JC = 2U - \dot{x}^2 - \dot{y}^2 - \dot{z}^2$.

Stability and Bifurcations In the circular restricted three-body problem, stability indices provide a useful measure of orbital stability. This metric is defined as

$$\nu_i = \frac{1}{2}\left(||\lambda_i|| + \frac{1}{||\lambda_i||}\right), \tag{2}$$

where λ_i represent the eigenvalues of the monodromy matrix, $\Phi(t+P,t)$, and P is the orbital period of the baseline orbit in the CR3BP.[5] Note that the eigenvalues of the monodromy matrix occur as two sets of reciprocal pairs and two trivial eigenvalues equal to unity. Thus, the set of eigenvalues from the monodromy matrix for a particular periodic orbit occur in the form: $(1,\ 1,\ \lambda_1,\ 1/\lambda_1,\ \lambda_2,\ 1/\lambda_2)$. If all of the stability indices are equal to unity, an orbit is linearly stable and possesses no unstable subspace; if any nontrivial stability index has magnitude greater than unity, the orbit is unstable and natural flow exists into and out of the orbit. The magnitude of the stability index is directly related to the rate of the departing/arriving flow. For example, the stability indices corresponding to the L_2 NRHOs range from 1 to 1.69, while the stability index for the halo orbit that bifurcates from the L_2 Lyapunov family is much larger at 606.11. For unstable orbits, a useful metric corresponding to the temporal scale of the dominant divergent motion is derived by considering the time constant, τ, as measured in terms of the number of revolutions along the nominal orbit, that is

$$\tau[\text{rev}] = \frac{1}{|\text{Re}(\ln(\lambda_{\max}(\Phi(t+P,t))))|}\frac{1}{P} \tag{3}$$

where $\lambda_{\max}(\cdot)$ is an operator that returns the largest magnitude eigenvalue of the argument matrix. Note that the time constant is infinite for a marginally stable orbit, i.e., $\lambda_{\max}(\Phi(t+P,t)) = 1$. The value $\tau[rev]$ is physically interpreted as the number of revolutions along the nominal orbit that are necessary to amplify a given initial perturbation in the dominant direction by a factor of e.[4] The time constant for the NRHOs ranges from approximately one revolution (for nearly stable orbits) to infinite revolutions (for stable NRHOs) while the time constant for the halo orbit that bifurcates from the L_2 Lyapunov family is much smaller at 0.0412 revolutions. The 9:2 synodic resonant L_2 NRHO has a time constant equal to 0.8751 revolutions.

Higher-Fidelity Ephemeris Model

For mission design applications where higher-fidelity modeling accuracy is required, N-body differential equations and planetary ephemerides are employed. In the ephemeris model, the motion of the particle of interest (e.g., a spacecraft), P_i, is rendered relative to a central body, P_q, in a frame described in terms of the inertially pointing axes $\hat{X}$-$\hat{Y}$-$\hat{Z}$. The particle P_i is influenced by the gravity of P_q as well as other perturbing particles, P_j. Such an N-body system is depicted in Figure 1. The well-known dimensional N-body relative vector equation of motion is written as

$$\ddot{\mathbf{r}}_{qi} = -G\frac{(m_i + m_q)}{r_{qi}^3}\mathbf{r}_{qi} + G\sum_{\substack{j=1 \\ j\neq i,q}}^{N} m_j\left(\frac{\mathbf{r}_{ij}}{r_{ij}^3} - \frac{\mathbf{r}_{qj}}{r_{qj}^3}\right) \tag{4}$$

where G denotes the universal gravitational constant, $m_{(\cdot)}$ is the mass of $P_{(\cdot)}$, and the definition of vector quantities is consistent with Figure 1. Note that a bold letter indicates a vector entity, while an identical non-bold symbol refers to the modulus of the corresponding vector. For this analysis, the relative position of each perturbing body with respect to the central body, $\mathbf{r}_{qj}$, is instantaneously computed by employing NASA's NAIF (Navigation and Ancillary Information Facility) SPICE ephemeris data. Since the operational trajectory for this specific analysis lies in close proximity to the Moon, selecting the Moon as a central body is reasonable and convenient for numerical integration. For this application, the mass m_q represents the Moon, the target mass, m_i, is the spacecraft, and the additional masses m_j correspond to additional bodies that exert a non-negligible gravitational attraction. The N-body vector differential equation is propagated in the J2000 inertial reference frame and includes the Earth, Moon, and Sun as celestial bodies of influence.

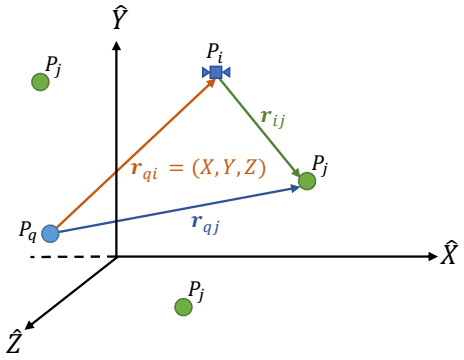

Figure 1: Geometry for an N-body system[6]

OVERVIEW OF DYNAMICAL STRUCTURES NEARBY THE L_2 NRHOS

In 2019, Zimovan-Spreen et al. identified periodic orbit families that bifurcate from the NRHO region along the family of L_2 halo orbits. Some of the periodic orbits in these families possess unstable and stable manifolds that are demonstrated to provide transfer options into and out of the NRHOs.[2,6] Some higher-order families that exist within the L_2 NRHO region are plotted in Figure 2.[2,6] These higher-order families possess members that are in resonance with the synodic period of the Moon. These synodic resonant orbits can be designed to avoid Earth and Moon shadows when transitioned to a higher-fidelity model.

LONG-DURATION ECLIPSE AVOIDANCE STRATEGIES

Mission constraints due to limitations on the spacecraft thermal environment and direct line-of-sight to Earth dictate allowable eclipse durations and frequencies.[3,7] Additionally, power requirements constrain the maximum time span for eclipsing events. Spacecraft moving in and nearby NRHOs are subject to both Earth eclipse and lunar eclipse conditions due to their proximity to both of these primary bodies. The NRHOs offer favorable eclipse avoidance properties due to their primarily out-of-plane orientation; the majority of the orbital motion is not coincident with the shadows of the Earth or Moon. However, duration of any passage through shadows must still be managed carefully.

Resonance Properties

Orbital resonance is an important consideration for meeting eclipse constraints. The NRHOs and various nearby orbits that are in resonance with the synodic period of the Moon are most often selected for applications due to the fact that avoiding and/or predicting eclipses is important to future missions. Resonance in terms of the synodic period is defined as the time between successive conjunctions of a celestial body with the Sun, i.e., the time required for the Earth-Moon-Sun orientation to repeat. In this case, a viewer fixed at the center of the Earth observes the Moon return to the same location with respect to the Sun after one synodic period of the Moon, however, the Moon does *not* appear in the same location to an observer in an inertial frame fixed at the center of the Earth. The Moon's synodic period is approximately 29.5 days, slightly longer

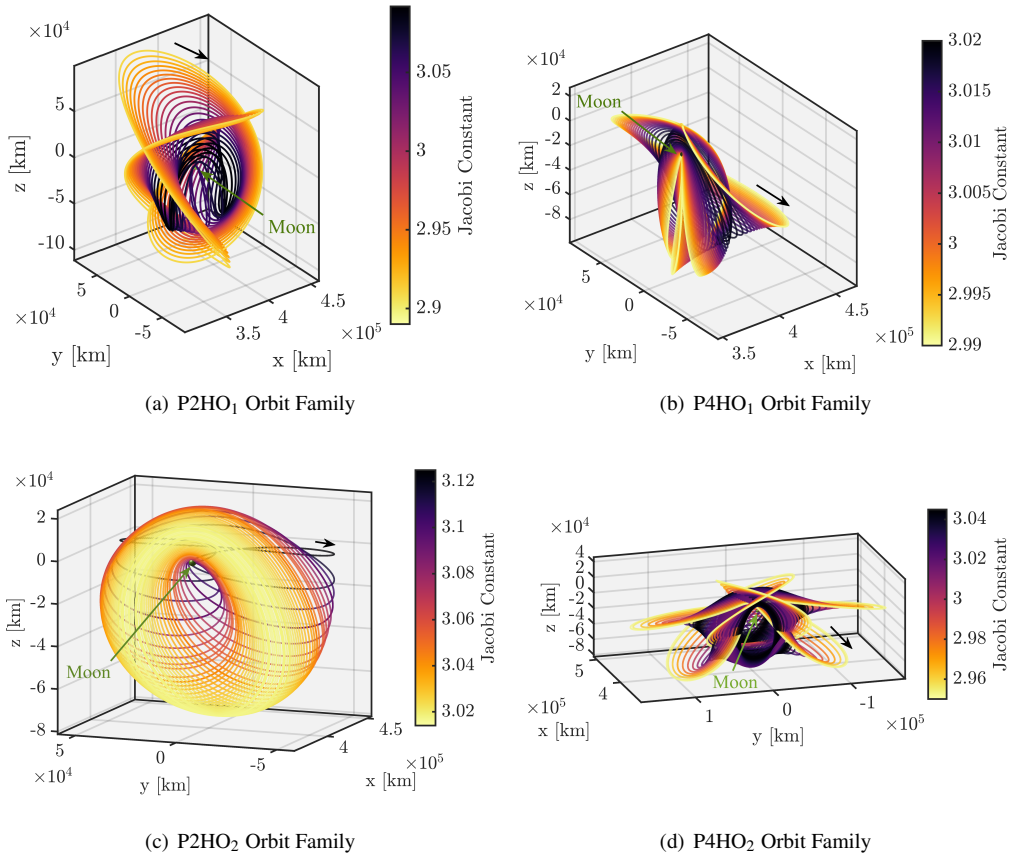

(a) P2HO$_1$ Orbit Family

(b) P4HO$_1$ Orbit Family

(c) P2HO$_2$ Orbit Family

(d) P4HO$_2$ Orbit Family

Figure 2: Sample families of periodic orbits that exist nearby the NRHO region of the L_2 Halo orbits.[2,6]

than its sidereal period (approximately 27.3 days). The synodic period is also denoted as a lunar month since the full lunar cycle (i.e., time between successive full Moon phases) requires one synodic period to complete.

Orbital resonance is defined in terms of a p:q ratio, where p indicates the number of completed revolutions of a given periodic orbit over q periods of the Moon. The value of p divided by q must be positive and rational, i.e., both p and q are written as positive integers. As an example of orbital resonance, a 4:1 synodic resonant NRHO possesses a period of approximately 7.375 days per revolution such that four revolutions of the spacecraft in this orbit are completed over the duration of one synodic period of the Moon ($7.375 * 4 = 29.5$). A 9:2 synodic resonant NRHO possesses a period of approximately 6.55 days such that nine revolutions along this orbit are completed over two synodic periods of the Moon. Figure 3 illustrates the 9:2 synodic resonant NRHO (plotted in orange) and the 4:1 synodic resonant NRHO (plotted in blue) computed in the CR3BP and plotted in the Earth-Moon rotating frame, the Moon-centered inertial frame, the Sun-Moon rotating frame, and the Sun-Earth rotating frame. In the inertial frame, these orbits do *not* appear as conics and are not periodic; note the shifting of the ascending node over each revolution. In the Sun-Moon and Sun-Earth rotating frames, gaps in the trajectory appear between the lobes of the orbit; in these frames, the geometry of p:q synodic resonant orbits repeats after q synodic periods. In Figure 4, the p:1 and p:2 synodic resonances for various L_2 halo orbits, as computed in the CR3BP, are plotted as a function of perilune radius.

Eclipse Avoidance Constraint Formulation

Transitioning a periodic orbit to an ephemeris model from the CR3BP presents challenges in maintaining a favorable geometry, especially for eclipse avoidance purposes. The NRHOs are particularly sensitive to this

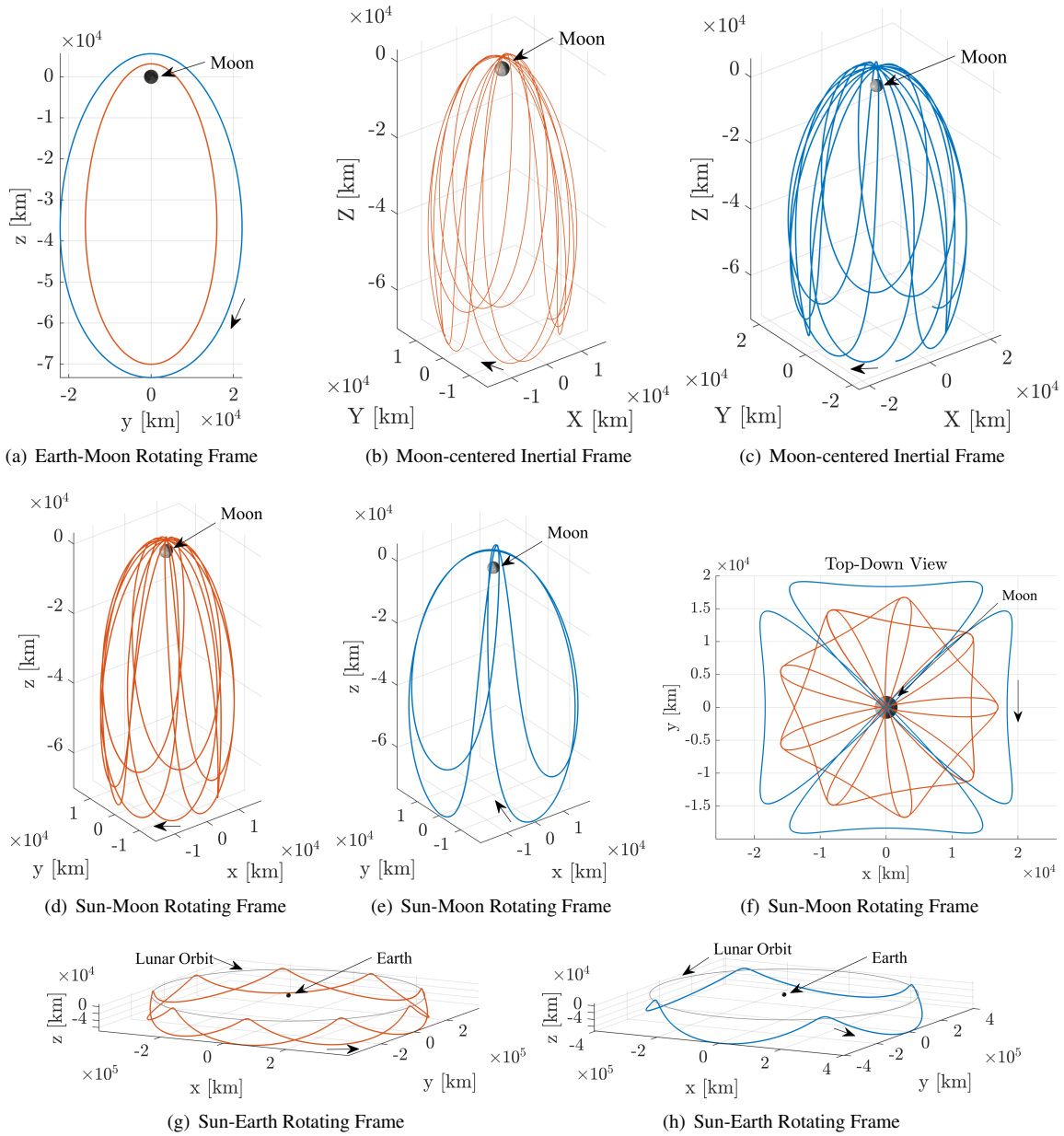

(a) Earth-Moon Rotating Frame (b) Moon-centered Inertial Frame (c) Moon-centered Inertial Frame

(d) Sun-Moon Rotating Frame (e) Sun-Moon Rotating Frame (f) Sun-Moon Rotating Frame

(g) Sun-Earth Rotating Frame (h) Sun-Earth Rotating Frame

Figure 3: The 9:2 synodic resonant NRHO (orange) and the 4:1 synodic resonant NRHO (blue) computed in the CR3BP

transition process.[8,9] A minimum norm targeting scheme allows a geometry that is maintained close by the CR3BP counterpart.[5] The initial epoch along the trajectory is selected such that the 'gaps' in the trajectory align with the Earth and lunar shadows, providing ballistic eclipse avoidance. The implementation of a constraint in the transition process between a lower-fidelity model and the ephemeris model further enables the generation of long-duration eclipse-free solutions.[10]

The addition of a path constraint, one that forces the trajectory to remain outside the shadows of the Earth and Moon, is one strategy that enables convergence of eclipse-free geometries in a higher-fidelity model.[10] The eclipse avoidance path constraint is based on the geometry of an occluding celestial body's shadow. Varying levels of shadow fidelity are available–a cone model is relatively simple and reasonably accurate.[11]

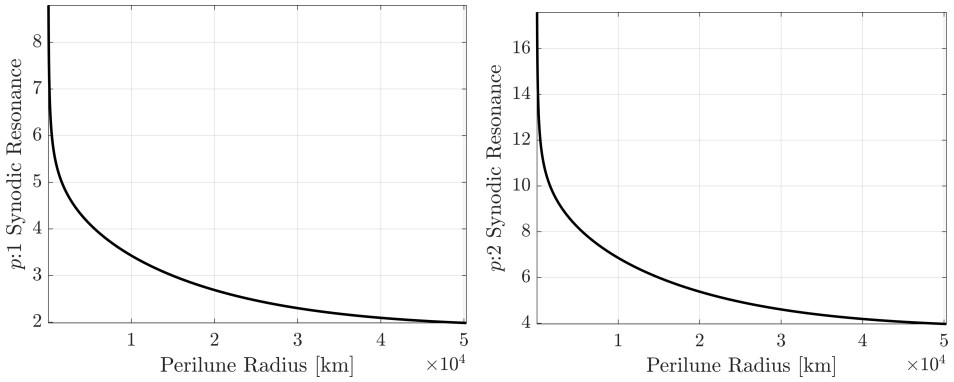

(a) p:1 Synodic Resonance (b) p:2 Synodic Resonance

Figure 4: Synodic Resonances within the L_2 Halo family[6]

Parameters to compute the shadow geometry are defined in Figure 5.[5] To compute the geometry of the shadow cone, multiple angles and distances are defined. In Figure 5, R is the radius of the Sun, S, r is the radius of the occluding body, O (the Earth or the Moon, i.e., the orange sphere), and r_{SO} is the distance between the Sun and the occluding body, at a given instant in time. Using geometry, the dimensions of the shadow cones are computed as

$$l = \frac{r * r_{SO}}{R - r} \tag{5}$$

$$p = \frac{r * r_{SO}}{R + r} \tag{6}$$

$$\alpha = \tan^{-1}\left(\frac{r}{p}\right) \tag{7}$$

$$\theta = \tan^{-1}\left(\frac{r}{l}\right) \tag{8}$$

Using these expressions and defining $\mathbf{r}_{Ssc}$ as the vector from the Sun to the spacecraft, $\mathbf{r}_{SO}$ as the vector from the Sun to the occluding body, and $\mathbf{r}_{Osc}$ as the vector from the occluding body to the spacecraft, the location of the spacecraft, sc, relative to the shadow is determined. The spacecraft is located within the penumbra if

$$r_{Osc}\sin(\zeta) \leq \left(p + \frac{\mathbf{r}_{SO}}{r_{SO}} \bullet \mathbf{r}_{Osc}\right)\tan\alpha \tag{9}$$

and

$$r_{Ssc} > r_{SO} \tag{10}$$

To avoid any eclipsing event, maintaining the spacecraft outside the penumbra is generally sufficient.

The mathematical expressions in Equations (9) and (10) are manipulated to formulate a path constraint for the ephemeris differential corrections multiple-shooting scheme;[5] this constraint, along with continuity constraints, guides the transition of periodic orbit trajectories between the CR3BP and the ephemeris model. The eclipsing path constraint is formulated as an expression, F_k, that is appended to the constraint vector for each of the segments, k, in the multiple-shooting scheme:[10]

$$F_k = \int_{\tau_k}^{\tau_k + T_{seg}} H(r_{Ssc} - r_{SO}) * (f - |f|)dt \tag{11}$$

where

$$f = r_{Osc}\sin(\zeta) - \left(p + \frac{\mathbf{r}_{SO}}{r_{SO}} \bullet \mathbf{r}_{Osc}\right)\tan(\alpha) \tag{12}$$

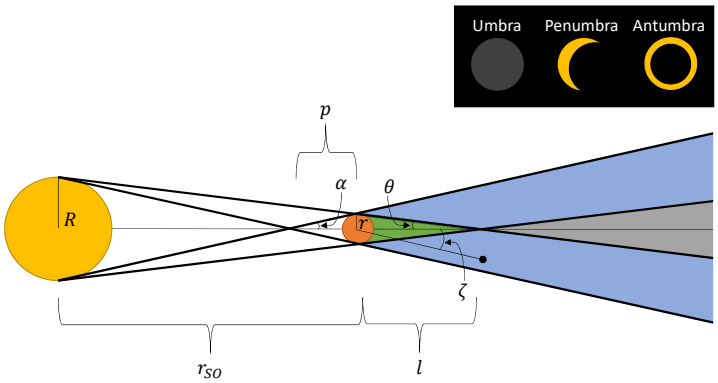

Figure 5: Eclipse Geometry Definitions

and $H(r_{Ssc} - r_{SO})$ is a Heaviside function used to turn the constraint 'on' when the spacecraft is located on the shadowed side of the occluding body from the Sun. The expression in Equation (11) is evaluated using a Riemann sum.

The path constraint formulation for eclipse avoidance is flexible and, thus, applicable in a variety of scenarios beyond long-duration eclipse-free baseline generation. As an example, this constraint proves useful in enforcing eclipse-free transfer trajectories between periodic orbits in cislunar space. In particular, the path constraint aids in designing solutions that meet mission constraints up-front, e.g., a spacecraft equipped with solar electric propulsion may not possess sufficient power to thrust while in shadow.

Eclipse Avoidance in the NRHOs

Some notable resonant NRHOs include the 9:2 and 4:1 synodic resonant orbits.[3] The 9:2 synodic resonant NRHO, possessing a perilune radius of approximately 3150 km and a period for each revolution of the orbit of about 6.5 days in the CR3BP, is currently selected as the baseline for NASA's Gateway architecture.[12] The 4:1 synodic resonant NRHO possesses a slightly higher perilune radius at 5600 km in the CR3BP. Due to the resonance properties of these orbits, epochs are available that avoid both Moon and Earth eclipses over long durations. The geometry of synodic resonant orbits in the Sun-Moon and Sun-Earth rotating frames easily illustrates the eclipse avoidance properties of resonant orbits. In each of these rotating frames, the shadow of the smaller body (i.e., the Moon or Earth) remains fixed along the respective positive x-axis. In these frames, the yz-projection of the trajectory is equivalent to a view looking down the shadow cone of the respective primary.

To illustrate the efficacy of synodic resonance in an eclipse avoidance scheme, an NRHO that does *not* possess a resonance with the synodic period of the Moon is illustrated in Figure 6. The period per revolution of this particular NRHO in the CR3BP is 7.52 days and the perilune radius is approximately 4571.7 km. This non-resonant orbit is nearby geometrically to both the 9:2 and 4:1 synodic resonant NRHOs, however, it is not fundamentally based upon predictable repeating behavior in the Sun-Earth and Sun-Moon rotating frames, as is evidenced by the trajectory plotted in Figures 6(b) through 6(f). Figure 6(d) illustrates the yz-projection of the trajectory included in the box in Figures 6(b) and 6(c) to clearly illustrate the trajectory crossing through the shadow of the Moon (note the depth of the projection as illustrated by the box). The yz-projection of the trajectory included in the box in Figure 6(e) is plotted in Figure 6(f) to visibly illustrate the passage of the trajectory through the Earth's shadow.

The 4:1 synodic resonant NRHO is plotted in Figure 7 in a variety of rotating frames. In Figure 7(a), the red periodic orbit demonstrates the 4:1 synodic resonant NRHO as computed in the CR3BP; the blue trajectory in this case corresponds to the higher-fidelity ephemeris trajectory, computed for 24 revolutions and plotted in the Earth-Moon rotating frame. The resonant geometry of this particular orbit is clearly apparent in Figures 7(b) through 7(f). In Figures 7(b) through 7(d), when the ephemeris trajectory is plotted in the Sun-Moon rotating frame, four distinct lobes are observed that correspond to the four revolutions of the trajectory over each lunar month. Figure 7(e) and 7(f) illustrate the trajectory in the Sun-Earth rotating frame; these

figures highlight four peaks and troughs corresponding to the perilune passes and apolune passes, respectively. Relatively wide gaps are observed across the lobes along the trajectory in the Sun-Moon rotating frame and the peaks along the trajectory in the Sun-Earth rotating frame. The size and orientation of these gaps allows for sufficient margin in eclipse avoidance and flexibility in the insertion epoch selection; the eclipse avoidance path constraint is not necessary to include for this particular epoch (initial apolune on December 30, 2020). The planar projections of the trajectory in the Sun-Moon rotating frame (Figures 7(c) and 7(d)) and in the Sun-Earth rotating frame (Figure 7(f)) illustrate the passage of the shadows of the Moon and Earth, respectively, through gaps in the trajectory. A 19 year pseudo-continuous eclipse-free solution, as constructed by Williams et al. in 2017, is available.[3]

A 9:2 synodic resonant NRHO, computed in the ephemeris model for 30 revolutions (approximately 6 months), is plotted in Figure 8 in the classical Earth-Moon rotating frame, Sun-Moon rotating frame, and Sun-Earth rotating frame. A similar pseudo-continuous fifteen year result is produced by Lee in work from 2019.[12] Figure 8(a) illustrates the 9:2 synodic resonant NRHO in the Earth-Moon rotating frame; the red trajectory is the CR3BP orbit, while the blue trajectory is computed in a higher-fidelity NAIF SPICE-based ephemeris model. Figures 8(b) through 8(e) illustrate the trajectory in the Sun-Moon rotating frame; in this frame there are nine lobes corresponding to the nine revolutions of the NRHO per two synodic periods of the Moon. The Moon's shadow passes primarily through a gap in the lobes, based on careful epoch selection (an epoch of January 9, 2020 is selected for the initial apoapsis), thereby avoiding most lunar eclipse events. The shadow passage through the gap between the lobes is apparent in the planar projections of the trajectory in Figures 8(c) through 8(e). In the case of the 9:2 synodic resonant NRHO, converging a continuous baseline in an ephemeris model using continuity constraints alone is *not* sufficient to guarantee an entirely eclipse-free baseline. Portions of the trajectory that pass through the shadow of the Moon are colored in magenta in Figures 8(b) through 8(e). The three shadow crossings along this trajectory that are clearly apparent in Figure 8(e), last approximately 25, 19, and 44 minutes, respectively. In Figure 8(f), in the Sun-Earth rotating frame, there are 9 peaks corresponding to the 9 perilune passes along the revolutions of the orbit; the Earth's shadow passes through a gap between these peaks and all Earth eclipse events are effectively avoided, as observed in the yz-projection of the trajectory in Figure 8(g). The lobes and peaks are approximately repeated after 9 revolutions due to the resonant period of the orbit with the lunar month.

Enforcing an eclipse avoidance path constraint in addition to a continuity constraint in the differential corrections process used to transition from the CR3BP to the ephemeris model yields a totally eclipse-free trajectory solution. Figure 9 illustrates 30 revolutions along a 9:2 synodic resonant NRHO that is free from lunar and Earth eclipsing events. The initial apolune along this trajectory, similar to the solution presented in Figure 8, has an epoch of January 9, 2020. A slight shift in the geometry of the trajectory, delivered through the enforcement of the eclipse-avoidance path constraint, yields an eclipse-free path. Note that in Figures 9(b) through 9(e), the trajectory does not pass through the lunar shadow. Small adjustments in the perilune radii and time required to complete each revolution produces a result that is eclipse-free over the path duration.

Eclipse Avoidance in Nearby Related Orbits

Some structures nearby the NRHOs are of particular interest for transfer design in the vicinity since they are unstable and, therefore, possess unstable and stable manifolds.[2] Since transfers into nearby higher-period orbits are likely to involve similar eclipsing constraints as those enforced for vehicles in NRHOs, it is useful to investigate the resonance properties of the nearby orbits as well. In Figure 10, the p:1 resonance is represented for each of the higher-period orbit families from Figure 2. Specific resonant solutions from the $P2HO_1$ (Figure 2(a)) and $P4HO_2$ (Figure 2(d)) families are investigated further due to their favorable long-duration eclipse avoidance properties. Depending on the mission application and the length of stay in a higher-period orbit, many other members of these families could be useful, however, they may not possess long-term eclipse avoidance geometries. The $P4HO_1$ and $P2HO_2$ families do not possess any simple p:q resonances that are defined in terms of $q = 1$ or $q = 2$. For higher-period orbits, such as those nearby the NRHOs, requiring multiple lunar months (i.e., $q > 2$) for resonance with the appropriate orbital period (i.e., an integer ratio between p and q) results in exceedingly complex geometries in the Sun-Moon and Sun-Earth rotating frames that, while relatively predictable, do not successfully avoid eclipses over a long time interval. Hence, periodic orbits in nearby families with p:1 and p:2 ratios that avoid eclipses for multiple revolutions are examined

further.

In Figure 10(a), it is apparent that 2:1, 1:1, and 3:2 (equivalently, $^3/_2$:1) synodic resonant orbits exist across the region of the P2HO$_1$ family nearby the NRHOs. It is inferred that the 2:1 synodic resonant P2HO$_1$ orbit possesses similar eclipse avoidance properties to that of the 4:1 synodic resonant NRHO. The full cycle of the P2HO$_1$ orbit includes two revolutions about the Moon while the full cycle for an NRHO includes one revolution about the Moon; therefore, the time required for one revolution about the Moon is commensurate between the 2:1 synodic resonant P2HO$_1$ orbit and the 4:1 synodic resonant NRHO. The 2:1 synodic resonant P2HO$_1$ orbit is illustrated in Figure 11 in three rotating frames. In the CR3BP, this butterfly orbit is defined with a perilune radius of 13967 km and a one revolution orbital period of 14.76 days. In Figure 11(a), the red orbit corresponds to the solution in the CR3BP, while the blue trajectory corresponds to 15 revolutions (221.3 days) of the orbit computed in the higher-fidelity ephemeris model. The familiar four lobes and four peaks (similar to those of the 4:1 synodic resonant NRHO) appear in Figures 11(b) through 11(f). Note that while the geometry differs slightly than the 4:1 synodic resonant NRHO, the general structure and eclipse avoidance properties are retained. The 2:1 synodic resonant P2HO$_1$ orbit is unstable with a maximum stability index of 12.31 (corresponding to a time constant equal to $\tau = 0.0919$ revolutions). Thus, these unstable orbits potentially possess useful manifold structures for transfer design.

In Figure 12, the 1:1 synodic resonant P2HO$_1$ is plotted in the Earth-Moon, Sun-Moon, and Sun-Earth rotating frames. The perilune radius for this orbit is 49986 km and the period of the orbit in the CR3BP (plotted in red in Figure 12(a)) is equal to the synodic period of the Moon, i.e., 29.5 days. Although the geometry of this orbit appears complex in the Earth-Moon rotating frame, the trajectory possesses a constant line of sight to Earth. Additionally, the 1:1 synodic resonant P2HO$_1$ ephemeris trajectory (plotted in blue) maintains a geometry similar to the CR3BP solution over many revolutions. This particular trajectory also possesses a very simple geometry in the Sun-Moon frame and Sun-Earth frame that leads to a straightforward eclipse avoidance scheme; the eclipse avoidance path constraint is not necessary to converge an eclipse-free baseline in the ephemeris model. In the Sun-Moon rotating frame, with the proper epoch selection, the shadow of the Moon passes directly through the large opening in the trajectory, as observed in Figures 12(b) and 12(c). Illustrated in Figure 12(d) and 12(e) in the Sun-Earth rotating frame, the Earth's shadow passes above a dip in the trajectory (corresponding to an apolune pass) and is successfully avoided along each revolution. The 1:1 synodic resonant P2HO$_1$ is unstable, as well, with a maximum stability index of 33.55 or time constant of $\tau = 0.03499$ revolutions; this orbit possesses unstable and stable spiral manifold structures that could offer utility for transfer design in the region.

The 3:2 synodic resonant P2HO$_1$ is plotted in Figure 13. In the CR3BP, this periodic solution possesses a perilune radius of 34970 km and a period of 19.67 days. In this case, an ephemeris solution corresponding to 295 days successfully avoids all lunar and Earth eclipses. The orbit is illustrated in the Earth-Moon rotating frame in Figure 13(a); note that the ephemeris solution (colored blue) does not vary greatly from the CR3BP counterpart (colored red). Similar to the 9:2 synodic resonant NRHO, the geometry of this solution in the Sun-Moon and Sun-Earth rotating frames is complex due to the fact that two lunar months are required to achieve an integer ratio with the period of the orbit, i.e., resonance, however, eclipses are still successfully avoided. Figures 13(b) through 13(d) illustrate the trajectory in the Earth-Moon rotating frame. The box plotted in Figures 13(b) and 13(c) illustrates the portion of the trajectory included in Figure 13(d); the depth of the projection in Figure 13(d) is consistent with the side length of the box in the x-direction in Figures 13(b) and 13(c). Similarly, the box included in Figure 13(e) highlights the projection of the trajectory in the Sun-Earth frame included in Figure 13(f). The maximum stability index for this orbit is 19.94 or, equivalently, the time constant associated with this orbit is $\tau = 0.05988$ revolutions. This particular P2HO$_1$ trajectory possesses stable and unstable spiral manifolds, possibly useful in transfer design into or out of the vicinity, for example, leveraging such flow to arrive at or depart from the NRHO.

Finally, in the P4HO$_2$ family, there is an orbit that possesses a 1:2 resonance with the synodic period of the Moon. For each single period or revolution along this orbit, the Earth-Moon-Sun orientation repeats twice (two lunar months). In Figure 14, three revolutions (or approximately half of a year) along the ephemeris trajectory are plotted in blue in various rotating frames. The CR3BP periodic solution appears in Figure 14(a) in red. A northern family member is plotted here since it more successfully avoids lunar eclipses

than its southern counterpart for this particular initial epoch and duration. The complex geometry of this trajectory does introduce some additional challenges in epoch selection as the margin across the available epochs for eclipse avoidance is not as wide as in trajectories with simpler geometries due to narrower gaps in the trajectory for the Earth and Moon shadows; this phenomenon is illustrated in Figures 14(b) through 14(e). Note that the box included in Figure 14(b) illustrates the depth of the yz-projection of the trajectory in Figure 14(c). The yz-projection clearly illustrates that the trajectory is not passing through the lunar shadow over the span of the trajectory plotted. The 1:2 synodic resonant $P4HO_2$ orbit possesses two unstable modes corresponding to invariant manifolds that approach/depart from this periodic orbit; this orbit does not possess a center subspace. The maximum linear stability index of this orbit is a notably large value at 36189.68, therefore, manifolds approach/depart from the vicinity of this trajectory rapidly, potentially offering utility for transfer design when the time-of-flight into and out of the lunar region is restricted. The time constant associated with this larger unstable mode is defined as $\tau = 0.006616$ revolutions.

CONCLUDING REMARKS

Near rectilinear halo orbits, the current baseline for NASA's upcoming Gateway mission, are linearly stable or nearly stable orbits in the lunar vicinity that possess useful eclipse avoidance properties. Due to the stable nature of these orbits, trajectory maintenance costs over a long duration are generally low, however, transfer trajectories into and out of the region are challenging to design and are potentially more costly due to a lack of useful ballistic pathways (i.e., manifolds) that lead to/from these orbits. Periodic structures in the vicinity, related to the NRHOs through period-multiplying bifurcations, offer additional insight into the nearby dynamical flow. These structures persist in a higher-fidelity ephemeris model. A long-term, low-cost solution to enforce eclipse duration constraints is necessary for spacecraft in NRHOs as well as the orbits in the surrounding vicinity–one solution is offered by considering orbits that possess resonance with the synodic period of the Moon. Some synodic resonant orbits within the NRHO region and the nearby higher-period orbits possess geometries that successfully avoid eclipses over a long time interval without re-phasing maneuvers along a baseline path. The enforcement of an eclipse-avoidance path constraint allows for the generation of eclipse-free solutions when a lunar synodic resonance-based geometry scheme alone does not suffice.

ACKNOWLEDGMENTS

The authors wish to thank the Purdue University School of Aeronautics and Astronautics for the facilities and support, including access to the Rune and Barbara Eliasen Visualization Laboratory. Additionally, the authors thank Sara Harris at NASA JSC for her insight. This research is supported by a National Aeronautics and Space Administration (NASA) Space Technology Research Fellowship, NASA Grant 80NSSC18K1153 as well as NASA Grant and Cooperative Agreement 80NSSC18M0122.

REFERENCES

[1] R. Whitley and R. Martinez, "Options for Staging Orbits in Cis-Lunar Space," *2016 IEEE Aerospace Conference*, 2016.

[2] E. M. Zimovan-Spreen and K. C. Howell, "Dynamical Structures Nearby NRHOs with Applications in Cislunar Space," *2019 AAS/AIAA Astrodynamics Specialist Conference*, Portland, Maine, August 11 – 15, 2019.

[3] J. Williams, D. E. Lee, R. L. Whitley, K. A. Bokelmann, D. C. Davis, and C. F. Berry, "Targeting Cis-lunar Near Rectilinear Halo Orbits for Human Space Exploration," *Paper No. AAS 17-267, AAS/AIAA Spaceflight Mechanics Meeting, San Antonio, Texas*, February 2017.

[4] E. M. Zimovan, K. C. Howell, and D. C. Davis, "Near Rectilinear Halo Orbits and Their Application in Cis-Lunar Space," *3rd International Academy of Astronautics Conference on Dynamics and Control of Space Systems*, Moscow, Russia, May 30 – June 1, 2017.

[5] E. M. Zimovan, "Characteristics and Design Strategies for Near Rectilinear Halo Orbits within the Earth-Moon System," M.S. Thesis, School of Aeronautics and Astronautics, Purdue University, West Lafayette, Indiana, August 2017.

[6] E. M. Zimovan-Spreen, K. C. Howell, and D. C. Davis, "Near Rectilinear Halo Orbits and Nearby Higher-Period Dynamical Structures: Orbital Stability and Resonant Properties," *Celestial Mechanics and Dynamical Astronomy*, Vol. 132, June 2020, DOI: https://doi.org/10.1007/s10569-020-09968-2.

[7] C. P. Newman, D. C. Davis, R. J. Whitley, J. R. Guinn, and M. S. Ryne, "Stationkeeping, Orbit Determination, and Attitude Control for Spacecraft in Near Rectilinear Halo Orbits," *Paper No. AAS 18-388, AAS Astrodynamics Specialist Conference, Snowbird, Utah*, August 2018.

[8] D. C. Davis, S. M. Phillips, K. C. Howell, S. Vutikuri, and B. P. McCarthy, "Stationkeeping and Transfer Trajectory Design for Spacecraft in Cislunar Space," *Paper No. AAS 17-826, AAS/AIAA Astrodynamics Specialist Conference, Columbia River Gorge, Stevenson, Washington*, August 2017.

[9] D. C. Davis, K. K. Boudad, R. J. Power, and K. C. Howell, "Heliocentric Escape and Lunar impact from Near Rectilinear Halo Orbits," *2019 AAS/AIAA Astrodynamics Specialist Conference*, Portland, Maine, August 11 – 15, 2019.

[10] J. A. Ojeda Romero and K. C. Howell, "Transfers from GTO to Sun-Earth Libration Orbits," *AAS/AIAA Astrodynamics Specialist Conference, Portland, Maine*, Portland, Maine, August 11–15, 2019.

[11] R. V. Robertson, *Highly Physical Solar Radiation Pressure Modeling During Penumbra Transitions*. Ph.D. Dissertation, Virginia Polytechnic Institude and State University, 2015.

[12] D. E. Lee, "White Paper: Gateway Destination Orbit Model: A Continuous 15 Year NRHO Reference Trajectory," Tech. Rep. Document ID: 20190030294, National Aeronautics and Space Administration, NASA Johnson Space Center, Houston, TX, August 20, 2019.

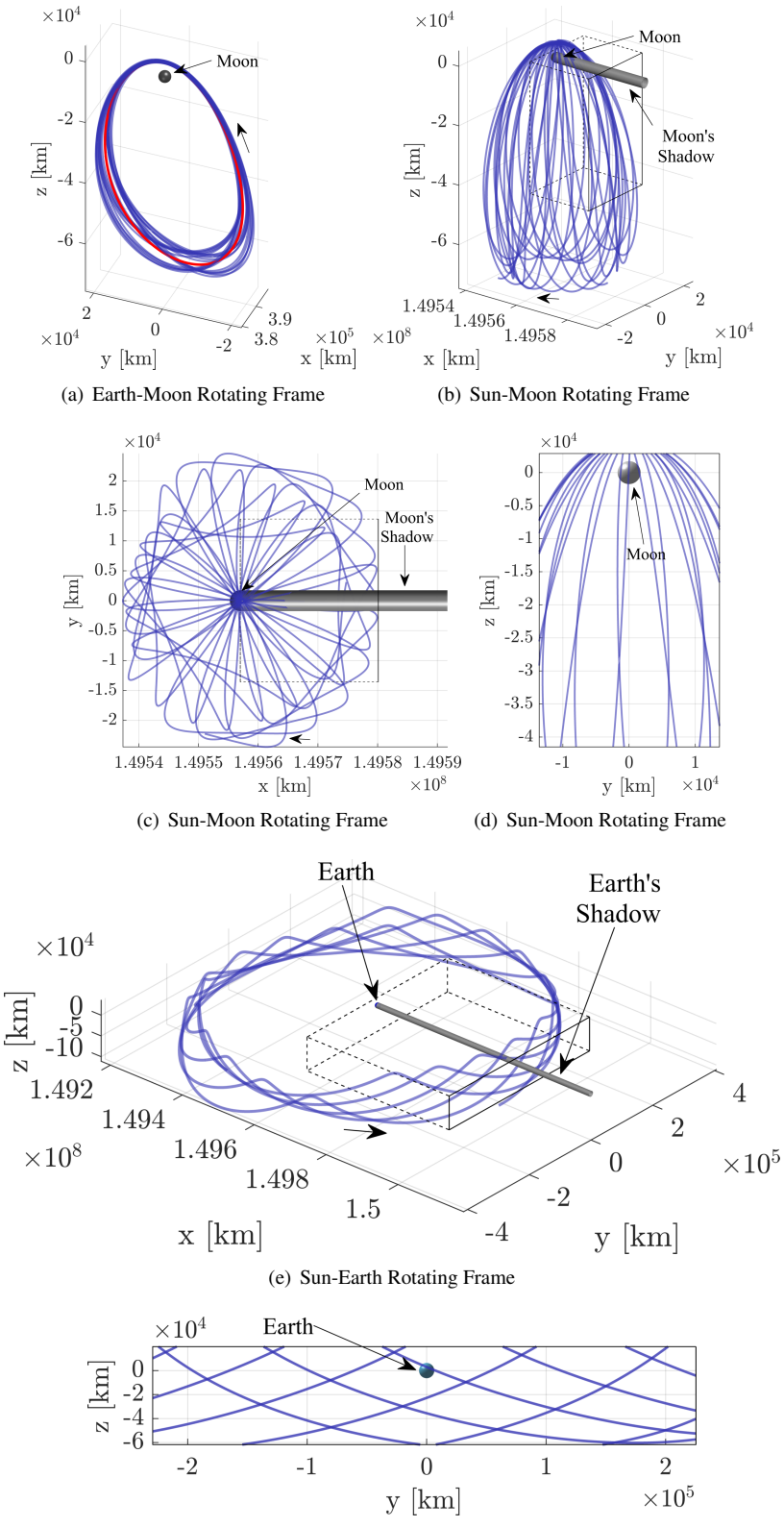

(a) Earth-Moon Rotating Frame

(b) Sun-Moon Rotating Frame

(c) Sun-Moon Rotating Frame

(d) Sun-Moon Rotating Frame

(e) Sun-Earth Rotating Frame

(f) Sun-Earth Rotating Frame

Figure 6: A Non-synodic Resonant NRHO in Various Rotating Frames[6]

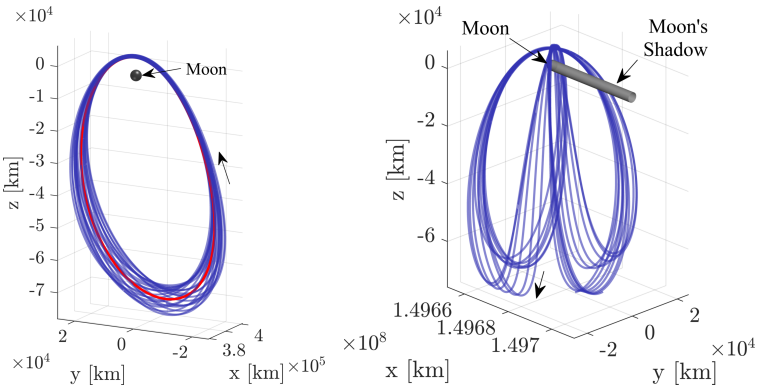

(a) Earth-Moon Rotating Frame

(b) Sun-Moon Rotating Frame

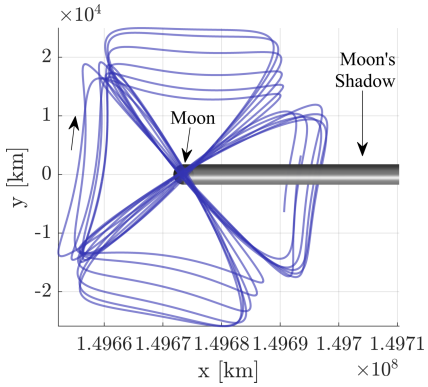

(c) Sun-Moon Rotating Frame

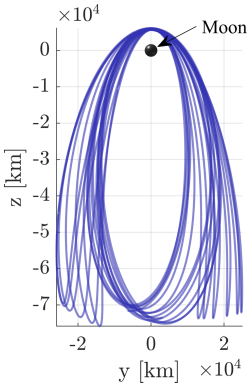

(d) Sun-Moon Rotating Frame

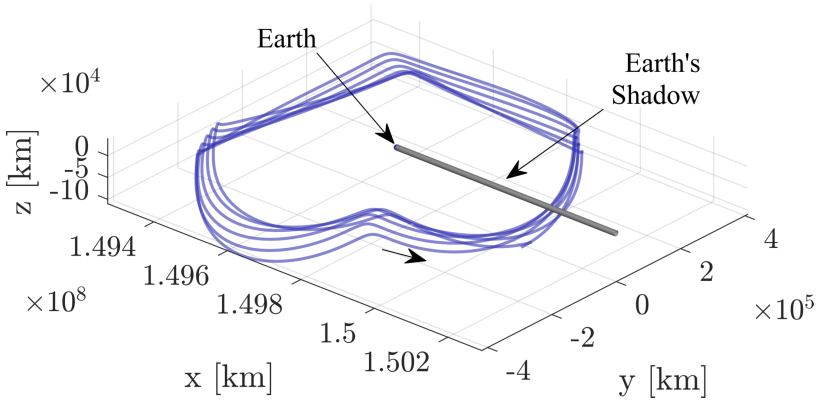

(e) Sun-Earth Rotating Frame

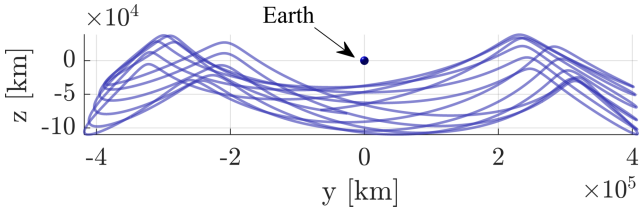

(f) Sun-Earth Rotating Frame

Figure 7: 4:1 Synodic Resonant NRHO in Various Rotating Frames[6]

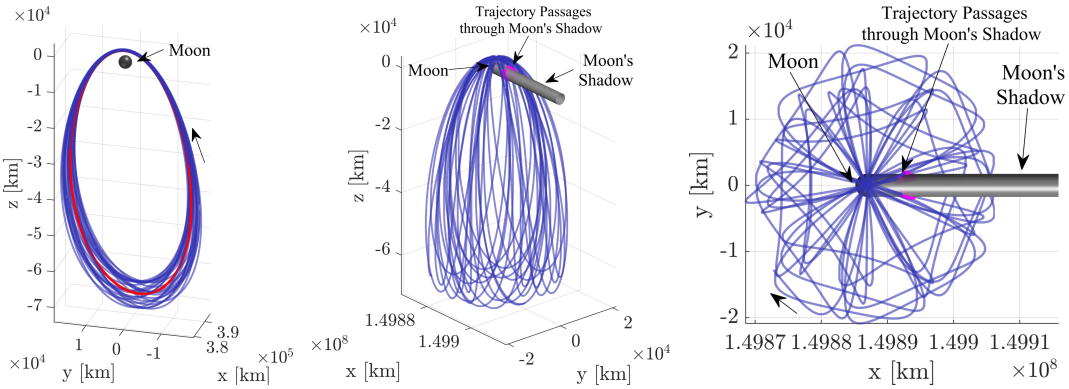

(a) Earth-Moon Rotating Frame (b) Sun-Moon Rotating Frame (c) Sun-Moon Rotating Frame

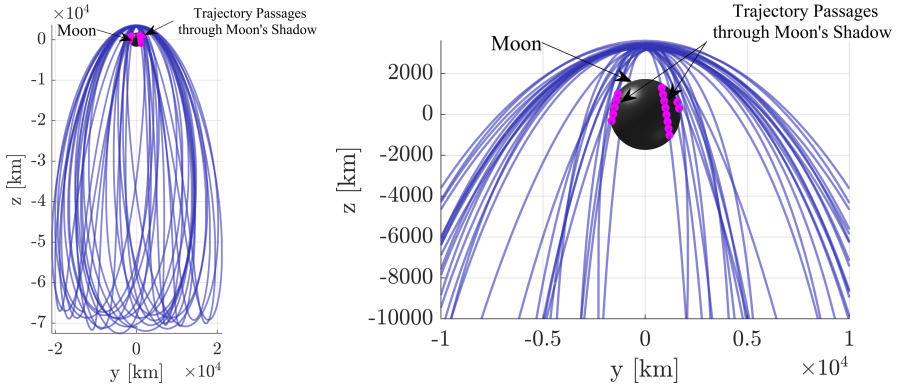

(d) Sun-Moon Rotating Frame (e) Sun-Moon Rotating Frame

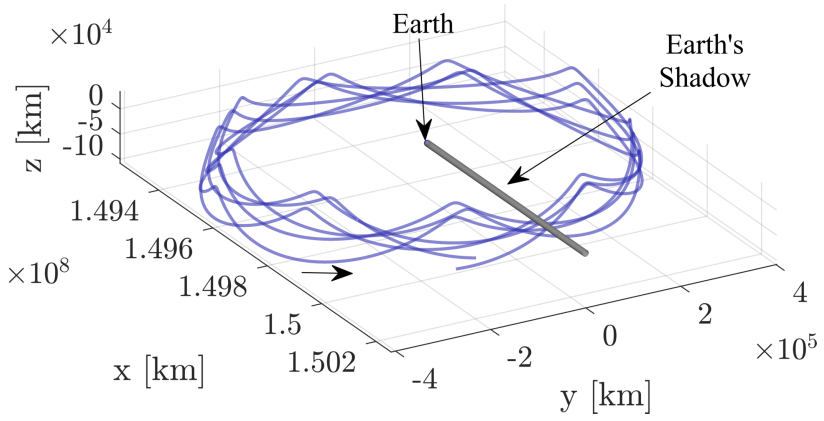

(f) Sun-Earth Rotating Frame

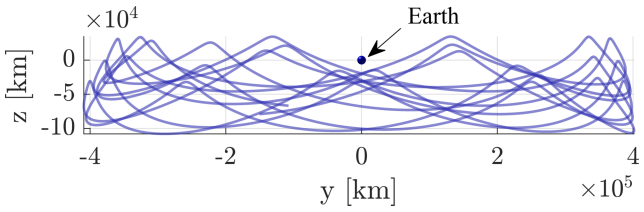

(g) Sun-Earth Rotating Frame

Figure 8: 9:2 Synodic Resonant NRHO in Various Rotating Frames;[6] The Eclipse Avoidance Constraint is Not Enforced

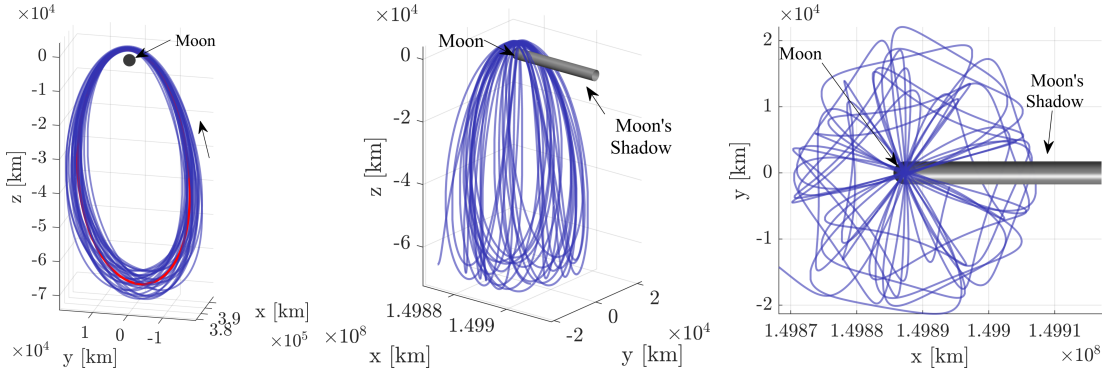

(a) Earth-Moon Rotating Frame (b) Sun-Moon Rotating Frame (c) Sun-Moon Rotating Frame

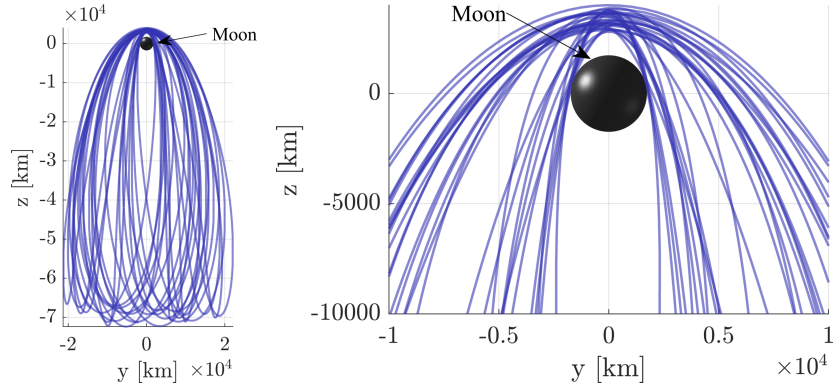

(d) Sun-Moon Rotating Frame (e) Sun-Moon Rotating Frame

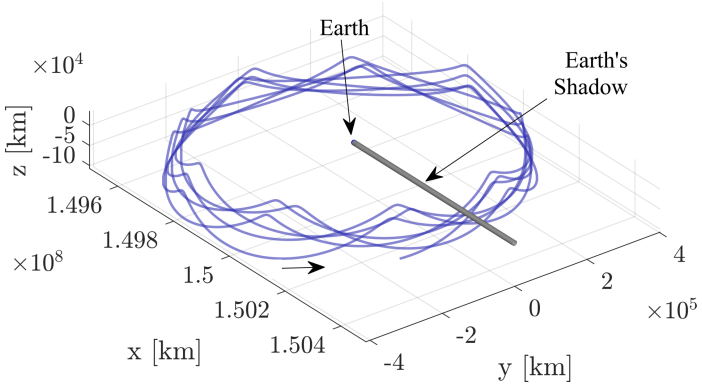

(f) Sun-Earth Rotating Frame

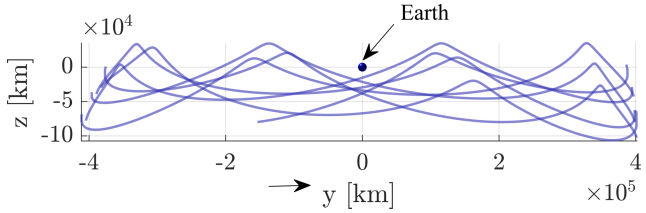

(g) Sun-Earth Rotating Frame

Figure 9: An Eclipse-Free 9:2 Synodic Resonant NRHO in Various Rotating Frames

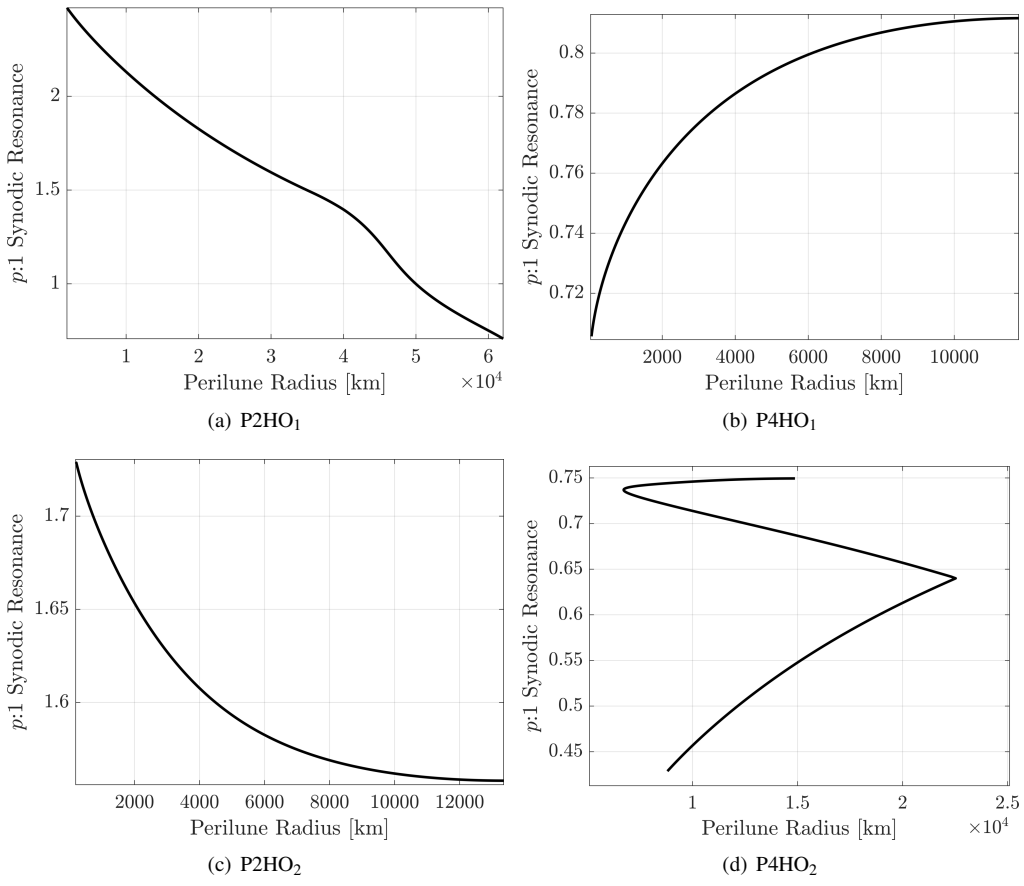

(a) P2HO$_1$ (b) P4HO$_1$

(c) P2HO$_2$ (d) P4HO$_2$

Figure 10: p:1 Synodic Resonance in Nearby Related Orbits[6]

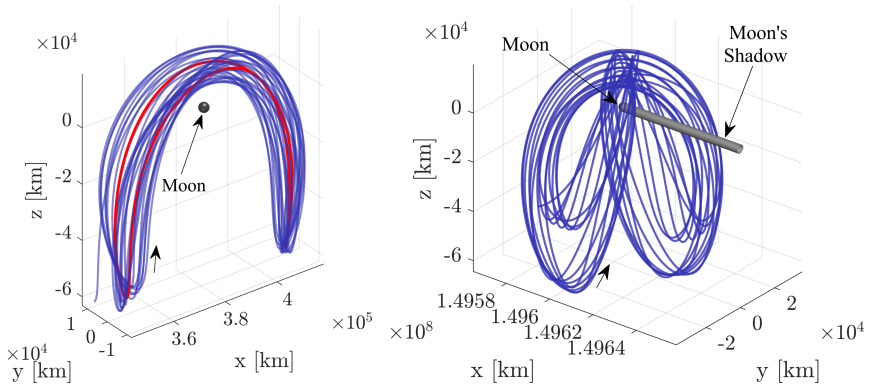

(a) Earth-Moon Rotating Frame

(b) Sun-Moon Rotating Frame

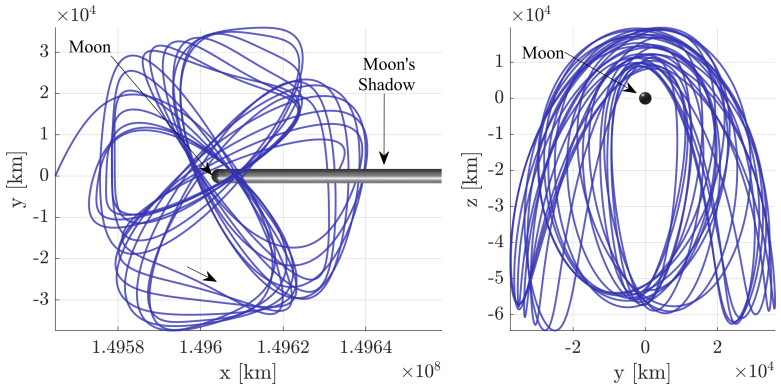

(c) Sun-Moon Rotating Frame

(d) Sun-Moon Rotating Frame

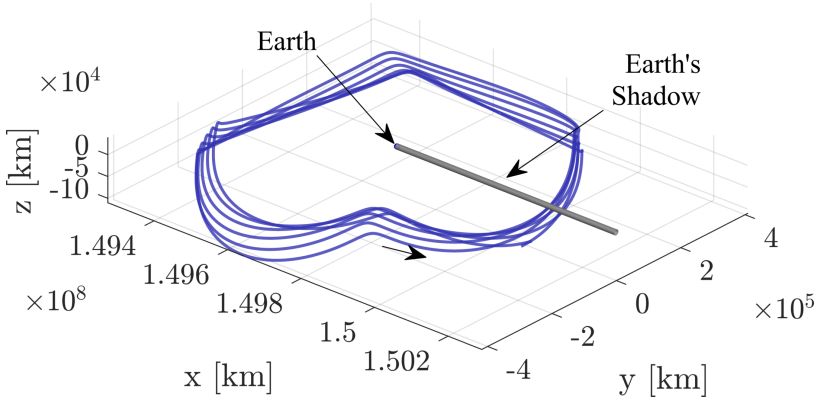

(e) Sun-Earth Rotating Frame

(f) Sun-Earth Rotating Frame

Figure 11: 2:1 Synodic Resonant P2HO$_1$ Orbit in Various Rotating Frames[6]

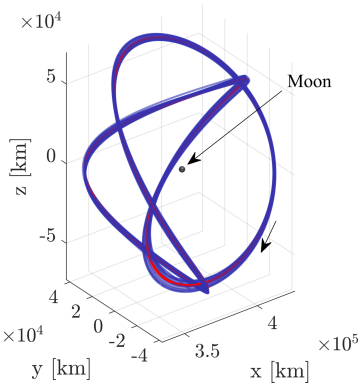

(a) Earth-Moon Rotating Frame

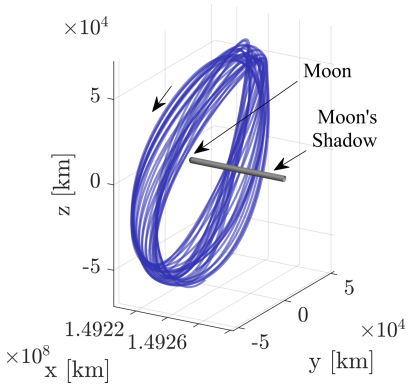

(b) Sun-Moon Rotating Frame

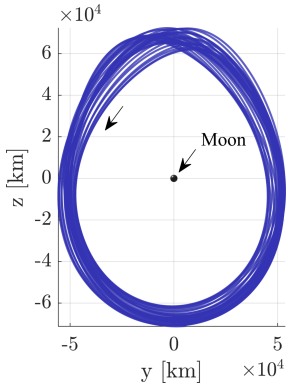

(c) Sun-Moon Rotating Frame

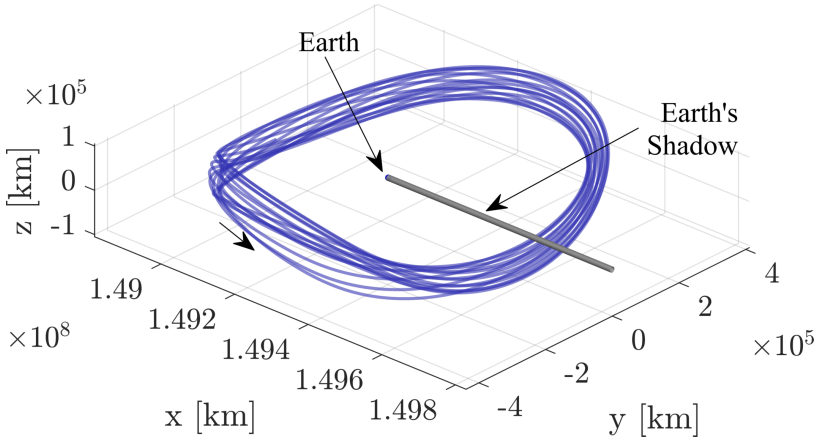

(d) Sun-Earth Rotating Frame

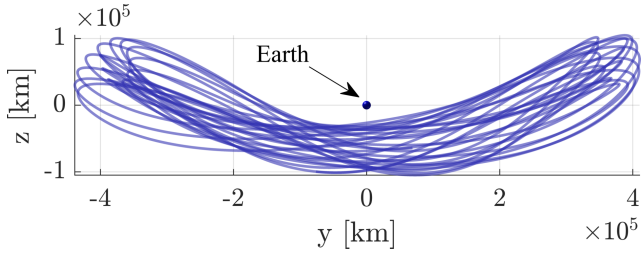

(e) Sun-Earth Rotating Frame

Figure 12: 1:1 Synodic Resonant P2HO$_1$ Orbit in Various Rotating Frames[6]

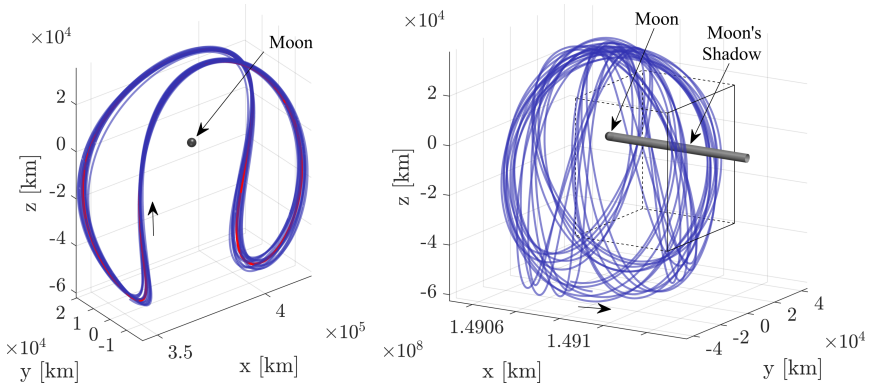

(a) Earth-Moon Rotating Frame (b) Sun-Moon Rotating Frame

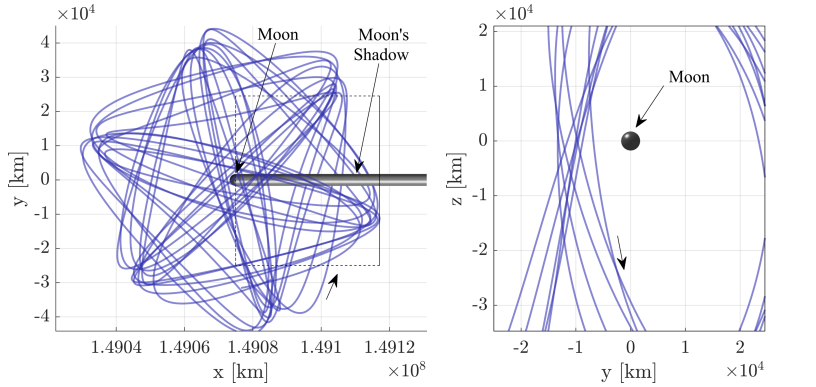

(c) Sun-Moon Rotating Frame (d) Sun-Moon Rotating Frame

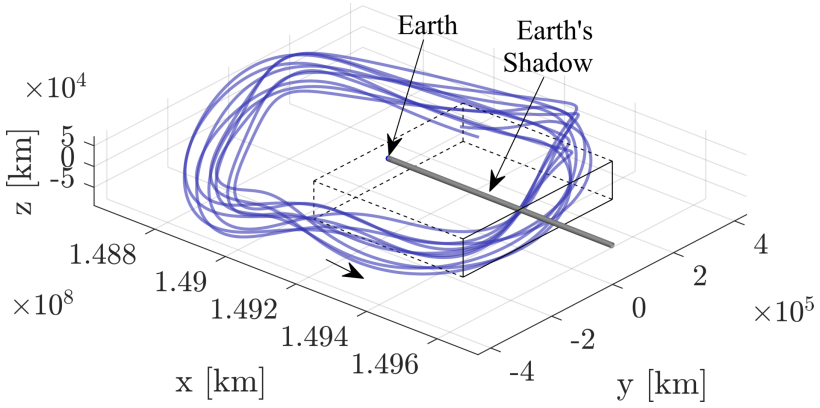

(e) Sun-Earth Rotating Frame

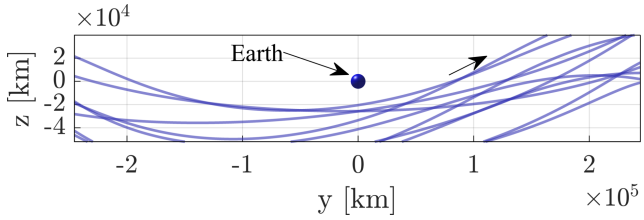

(f) Sun-Earth Rotating Frame

Figure 13: 3:2 Synodic Resonant P2HO$_1$ Orbit in Various Rotating Frames[6]

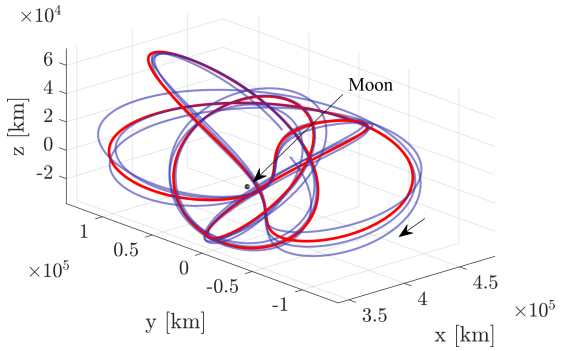

(a) Earth-Moon Rotating Frame

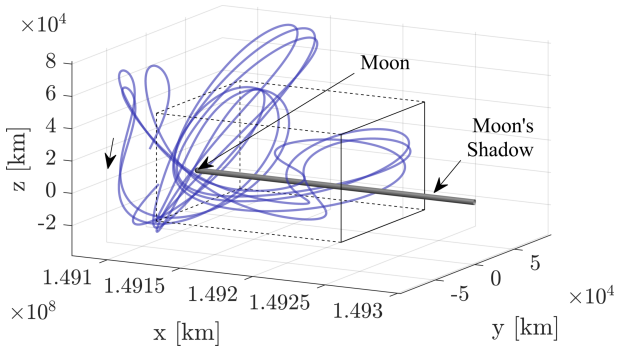

(b) Sun-Moon Rotating Frame

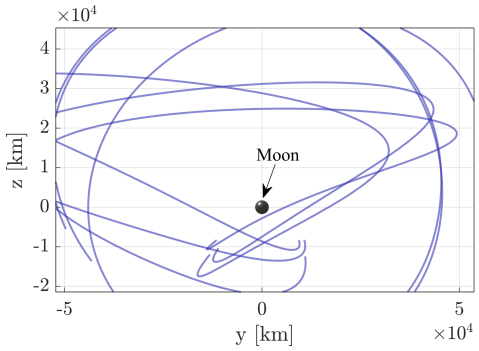

(c) Sun-Moon Rotating Frame

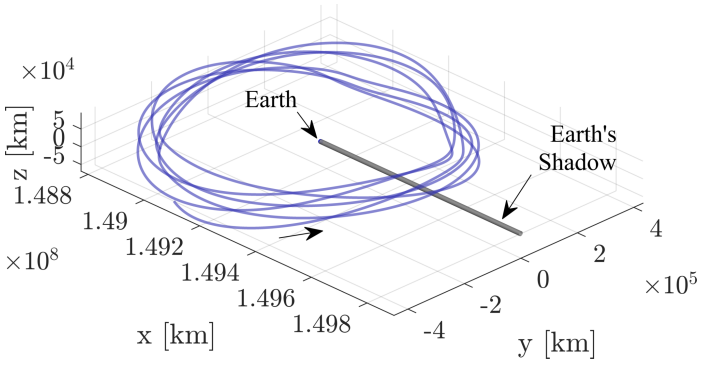

(d) Sun-Earth Rotating Frame

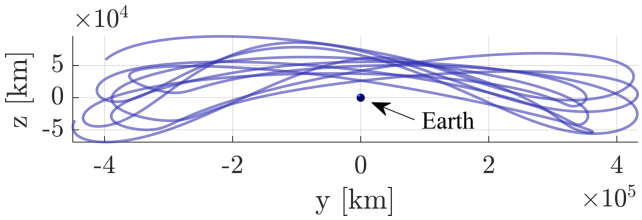

(e) Sun-Earth Rotating Frame

Figure 14: 1:2 Synodic Resonant Northern P4HO$_2$ Orbit in Various Rotating Frames[6]